C54-TiSi_2 formation using nanosecond laser annealing of A-Si/Ti/A-Si stacks

Réda Guelladress, Sébastien Kerdilès, Mélanie Dartois, Chiara Sabbione, Magali Gregoire, Dominique Mangelinck

C54-$TiSi_2$ FORMATION USING NANOSECOND LASER ANNEALING OF A-Si/Ti/A-Si STACKS

Réda Guelladress[1,2,3,*] , Sébastien Kerdilès[2], Mélanie Dartois[2], Chiara Sabbione[2], Magali Gregoire[1] and Dominique Mangelinck[3]

[1]STMicroelectronics, 850, rue Jean Monnet, 38920, Crolles cedex, France

[2]Université Grenoble Alpes, CEA-LETI, F-38000 Grenoble, France

[3]Aix Marseille Univ, CNRS, IM2NP, Case 142, Fac. Saint Jérôme, 13397 Marseille Cedex 20, France

* Corresponding author: STMicroelectronics, 850, rue Jean Monnet, 38920, Crolles cedex, France.

E-mail address: reda.guelladress@im2np.fr (R. Guelladress)

ABSTRACT

Low resistive Ti-based contacts are required to reach the targeted performances of 3D imaging devices. To fulfill this request, the C54-$TiSi_2$ phase appears to be the most efficient. However, in view of monolithic integration, the temperature needed to form C54-$TiSi_2$ must be drastically reduced by at least 100 °C in order to avoid damage in other parts of the device. Indeed, as these 3D imaging devices require the co-integration of Ti and Ni based silicides, it is crucial to develop a thermal treatment which allows to form the C54-$TiSi_2$ phase without agglomerating the NiSi layer (i.e. at temperatures lower than 600 °C). In this work, a three-layer stack made of a Ti layer in between two amorphous Si thin films deposited on (100) Si substrate has been studied. Nanosecond laser annealing (NLA) followed by rapid thermal annealing (RTA) from 500 to 800 °C were performed on those stacks. Sheet resistance and X-Ray Diffraction measurements showed that the C54-$TiSi_2$ phase could be formed with a RTA treatment at a temperature as low as 600 °C in this case. In line with some previous work, this was due to another phase sequence involving the C40-$TiSi_2$ during the laser annealing. The most favorable microstructure to form C54-$TiSi_2$ by a subsequent RTA treatment seemed to be a matrix made of amorphous titanium silicide containing

grains of the C40-$TiSi_2$ template phase. This hypothetical microstructure was formed by laser annealing at a lower energy density when layers of amorphous Si were used.

Keywords:

C40-$TiSi_2$; C54-$TiSi_2$; thermal treatment; Ultra-Violet Nanosecond Laser Annealing; amorphous titanium silicide.

1. Introduction

Silicides are widely used as contacts in microelectronics devices. In the early 2000s, $TiSi_2$ silicides were massively replaced by $CoSi_2$ thin films in Complementary Metal Oxide Semiconductor (CMOS) technologies because of several issues including the narrow lines effect [1]. More recently, as device dimensions kept decreasing, $CoSi_2$ was replaced by NiSi [1].

Recently, titanium silicide has been re-introduced as a contact layer on top of photodiodes and transfer gates of CMOS image sensors, as well as in the sources/drains of 3D fin-type Field Effect Transistors, to reach high devices performances [2-11]. For those applications, titanium silicide is formed using a “SAlicide last” process (SAlicide = Self-Aligned silicide) [12] with only one Rapid Thermal Annealing (RTA) at a temperature between 600 and 850 °C.

In 3D monolithic image sensors, TiSi-based contacts are fabricated after the formation of a very thin Ni(Pt)Si layer. The agglomeration of the Ni(Pt)Si layer, eventually due to too high a thermal budget during RTA, is a major concern because it can lead to device degradation [13]. As recently reported, the typical threshold temperature for the agglomeration of those films is, in real devices, around 550 °C [14-15]. The effective agglomeration temperature for devices is thus 50 °C lower than the one reported by several groups for blanket wafers [16-25]. Indeed, nickel silicide layers usually agglomerate around 600 °C [16-25]. The co-integration of both silicide layers on the same wafer would require an increase of the Ni(Pt)Si agglomeration temperature, and/or a reduction of the formation temperature of the low-resistivity $TiSi_2$ phase. Several paths are emerging [26-34]. One of them, which was evaluated within the frame of monolithic 3D integration, is the use, prior to classical RTA, of an Ultra-Violet Nanosecond Laser Annealing (UV-NLA) to reduce the formation temperature of C54-$TiSi_2$ by modifying the usual phase sequence in which the C54-$TiSi_2$ phase nucleates from the C49-$TiSi_2$ phase [35-44]. Those studies showed that laser annealing resulted in the appearance of a C40-$TiSi_2$ phase that promoted the formation of the C54-$TiSi_2$ during a subsequent annealing. These three phases (C40-$TiSi_2$, C49-$TiSi_2$ and C54-$TiSi_2$) have different crystalline structures and resistivities. The C49-$TiSi_2$ phase has an orthorhombic base centered structure and a resistivity of 50-70 µΩ.cm [42]. The low resistivity phase is the C54-$TiSi_2$ phase, with an orthorhombic face centered structure and a resistivity of 15-20 µΩ.cm [42]. The C40-$TiSi_2$ phase, a template phase which favors the C54-$TiSi_2$ phase formation compared to the C49-$TiSi_2$ phase, has a hexagonal structure and a resistivity of 35 µΩ.cm [42]. Esposito et al. [42] found that a laser annealing at 0.85 J/cm² enabled the formation of the C54-$TiSi_2$ phase using a subsequent RTA at 650 °C instead of 800 °C. With such a UV-NLA, the first step in the phase sequence was the formation of a microstructure made of a matrix of amorphous silicide with grains of C40-$TiSi_2$ phase [42-44].

The use of amorphous silicon obtained by Pre-Amorphizing Implantation (PAI) has otherwise been studied to form titanium silicide [26-31]. Antimony PAI helped reducing the temperature

transformation of the C49-$TiSi_2$ phase into the C54-$TiSi_2$ phase [27,31]. Arsenic PAI yielded smaller grains of the C49-$TiSi_2$ phase, resulting in C54-$TiSi_2$ formation in reduced dimensions [27,29-30]. These results paved the way for investigations on the impact of Si crystallinity on the formation of titanium silicide intermediate phases [25-44].

In the present paper, the titanium silicide formation is studied by applying UV-NLA then RTA on a three-layer stack made of a Ti layer in between two amorphous Si (a-Si) layers. More precisely, samples were from top to bottom: TiN (capping layer) / a-Si / Ti / a-Si / (100) Si (substrate). Our aim was to form C54-$TiSi_2$ with a reduced thermal budget than without the presence of those a-Si layers sandwiching the Ti layer. The different phases formed after laser annealing then RTA treatment were evaluated by Sheet Resistance (Rs), Time-Resolved Reflectivity (TRR), Scanning Electron Microscopy (SEM), Transmission Electron Microscopy (TEM), Energy Dispersive Spectroscopy (EDX) and X-ray Diffraction (XRD). The comparison between stacks containing a-Si and reference samples made of TiN / Ti / (100) Si is discussed in terms of phases formation and thermal budget.

2. Experimental details

Prior to deposition, 300 mm diameter Si(100) substrates were cleaned using a solution of hydrofluoric acid. For all samples, layers were deposited in a Physical Vapor Deposition (PVD) tool under an argon atmosphere at 70 °C. Schematics of the samples are provided in Figure 1. For the reference sample, a layer of Ti (10 ± 1 nm) was deposited by PVD on the c-Si substrate while, for the multilayer stack, the Ti layer was embedded in between two a-Si layers with the same thickness (10 ± 1 nm). The a-Si layers were also deposited using PVD in an argon atmosphere at 70 °C. On both types of samples, a capping layer of TiN (15 ± 1 nm) was then deposited by PVD.

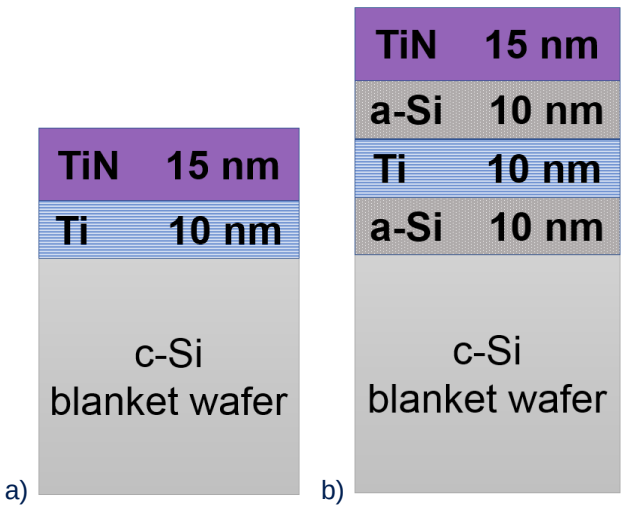

Figure 1 *: Schematics of the as-deposited stacks: a) reference samples b) multilayer sample. All layers were deposited by PVD.*

All samples were then annealed in an UV-NLA tool, more precisely in a SCREEN LT3100 platform which uses a XeCl laser (wavelength: λ = 308 nm, full width at half maximum of the pulse: τ = 160 ns), under a N_2 atmosphere. The laser beam exhibits a “top hat” shape and a 15 x 15 mm² size with a homogeneity better than 2.5 % within each field exposed to the laser (same size as the beam). Figure 2 shows the UV-NLA mapping on each wafer. Four series of annealed areas were irradiated by 1, 2, 3 or 10 pulses at the same location, with an increasing energy density (ED) ranging from 0.3 to 1.0 J/cm² with 0.025 J/cm² steps. Exposed fields were separated one of the other by 3 mm wide non-irradiated bands.

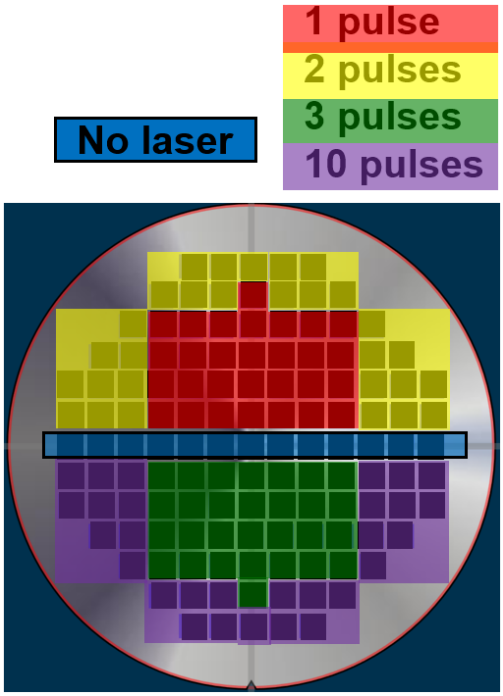

Figure 2 *: UV-NLA map on each 300 mm wafer.*

In-situ time-resolved reflectivity (TRR) was also performed during UV-NLA in the SCREEN LT-3100 tool. Meanwhile, Rs measurements, SEM and TEM observations were conducted after laser annealing. In addition, EDX profiles were collected for each TEM image.

Cumulative RTAs, named hereafter c-RTA, were performed after UV-NLA. They consisted in successive RTA performed on the same samples from 500 to 800 °C with 50°C steps. All RTAs were performed under N_2 during 30s in a Levitor 4300 system from Levitech. After each RTA, sheet resistances measurements were performed using a WS3000 tool from NAPSON, using 4-point probes with 1 mm spacing. SEM top view observations were carried out using a SEM Vision platform from Applied Materials, in the secondary electrons imaging mode with a 1000 V acceleration voltage. After thermal treatments (UV-NLA or UV-NLA + c-RTA), θ-2θ XRD measurements were performed at 1.541 Å (Cu Kα) in an Empyrean tool. Some of these samples were also characterized by TEM-EDX using a Tecnai Osiris tool from Thermofisher using an

operating voltage of 200 kV. The preparation of these samples is made using a plasma Focused Ion Beam (FIB) tool from Thermofisher

3. Results

3.1 Reference : TiN / Ti / (100) Si samples

a)

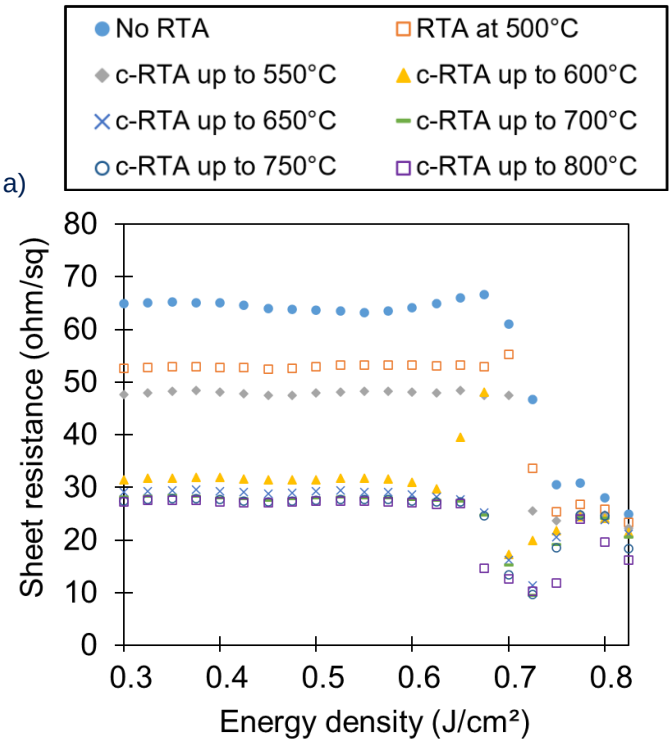
No RTA
RTA at 500°C
c-RTA up to 550°C
c-RTA up to 600°C
c-RTA up to 650°C
c-RTA up to 700°C
c-RTA up to 750°C
c-RTA up to 800°C
Sheet resistance (ohm/sq)
80
70
60
50
40
30
20
10
0
0.3
0.4
0.5
0.6
0.7
0.8
Energy density (J/cm²)

b)

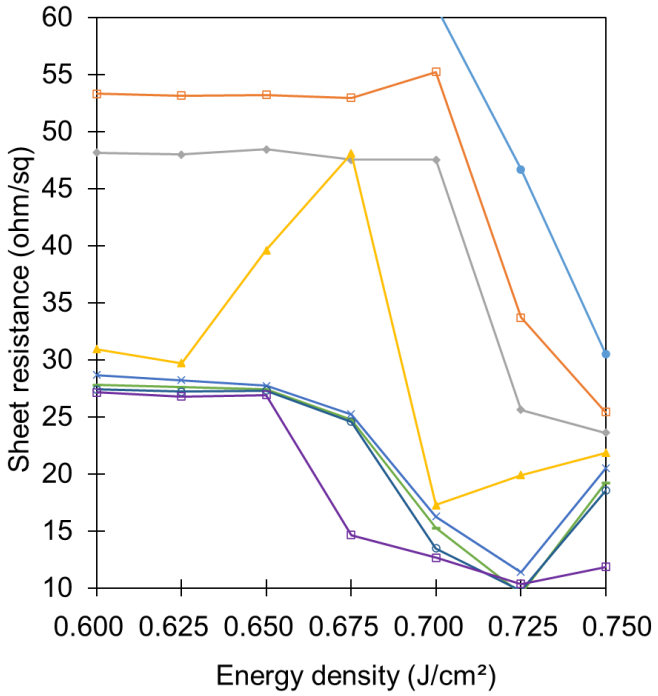
Sheet resistance (ohm/sq)
60
55
50
45
40
35
30
25
20
15
10
0.600
0.625
0.650
0.675
0.700
0.725
0.750
Energy density (J/cm²)

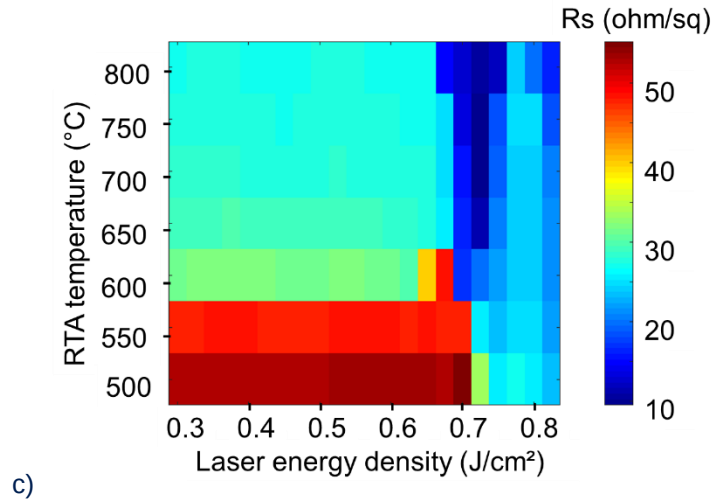

c)

Figure 3 *: Sheet resistance of the reference sample (TiN 10 nm / Ti 11 nm / (100) Si) samples after 3 UV-NLA pulses with an energy density between 0.3 J/cm² and 0.825 J/cm² (steps of 0.025 J/cm²) followed by c-RTA at temperatures between 500 and 800 °C. a) Evolution over the full range (graph with markers). b) Zoom (lines and markers) on the Rs decrease between 0.600 and 0.750 J/cm². c) 2D color map. Each rectangle corresponds to a given energy density as well as a given temperature and its color corresponds to the sheet resistance value.*

Figure 3 shows Rs measurements on TiN/Ti/ (100) Si samples after 3 UV-NLA pulses and successive RTAs. After 3 UV-NLA pulses without any RTA, Rs is stable around 65 Ω/sq for ED values lower than 0.625 J/cm² (blue circles). Between 0.625 J/cm² and 0.675 J/cm², Rs increases slightly to a maximum of 68 Ω/sq. Between 0.700 J/cm² and 0.750 J/cm², Rs drops to 30 Ω/sq. For EDs higher than 0.750 J/cm², Rs slowly decreases to 25 Ω/sq.

When a subsequent RTA is applied at 500 °C and 500 + 550 °C, Rs remains stable at relatively high values, around 50 Ω/sq, for low UV-NLA energy densities (e.g. lower than 0.600 J/cm²), as seen in Fig. 3a with orange squares and grey diamonds. For c-RTA at temperatures between 600 and 800 °C (yellow triangles, blue crosses, green dashes, unfilled blue circles and unfilled purple squares), the Rs plateau is around 30 Ω/sq for low UV-NLA energy densities. For c-RTA up to 600 °C, there is a Rs increase between 0.650 – 0.675 J/cm², and then, a strong decrease at 0.700 J/cm² followed by another increase as ED becomes higher. For c-RTA at 650 °C and above, Rs drops at 0.675 J/cm² and reaches a minimum around 10 Ω/sq for ED = 0.700-0.750 J/cm² as seen in Fig. 3b. For higher EDs, Rs increases back to approximately 20 Ω/sq. These behaviors are clearly evidenced in the color map (Figure 3c) and especially: (i) the sharp Rs decrease at 0.675-0.725 J/cm² for c-RTA temperatures between 550 and 650 °C, and (ii) the low Rs valley centered around 0.700 J/cm² for c-RTA temperatures from 650 up to 800 °C. In addition, the XRD diffractograms collected on TiN / Ti samples submitted to 3 UV-NLA pulses at various ED values and a c-RTA up to 800 °C are shown in Figure 4.

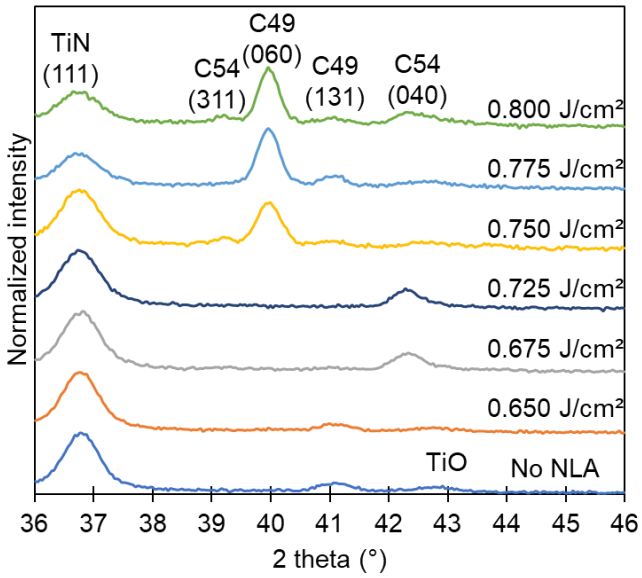

Figure 4 *: 2θ-θ XRD scans for TiN / Ti / c-Si samples after 3 UV-NLA pulses (ED between 0.650 J/cm² and 0.800 J/cm²) followed by c-RTA up to 800 °C. The curve labelled 'No NLA' corresponds to a sample not submitted to UV-NLA but annealed only with c-RTA up to 800 °C.*

In all cases, the peak at 36.7 ° corresponds to TiN (111). For samples with only a c-RTA up to 800 °C ('No NLA') or with a low ED laser annealing (e.g. ED ≤ 0.650 J/cm²) prior to c-RTA, the C49-$TiSi_2$ phase was the only silicide phase detected, with a (131) peak at 41.1 °. Given the thermal treatment, the C54-$TiSi_2$ phase was expected [42]. This might be due to the presence of oxygen that got into the sample during PVD.

For UV-NLA with EDs between 0.675 and 0.725 J/cm² followed by c-RTA up to 800 °C, the C54-$TiSi_2$ (040) peak was observed. At 0.750 J/cm² or above, the C49-$TiSi_2$ (060) appeared at 40.0 °. Then, at a higher ED, the C49-$TiSi_2$ (060) peak was the main one. C49-$TiSi_2$ (131) and C54-$TiSi_2$ (040) and (311) peaks were also detected, although they were less intense.

3.2 a-Si/Ti/a-Si stacks

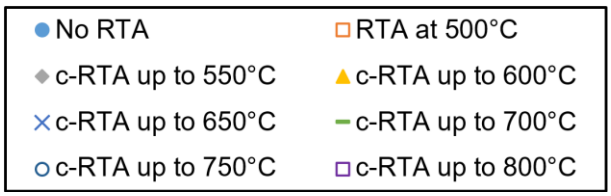

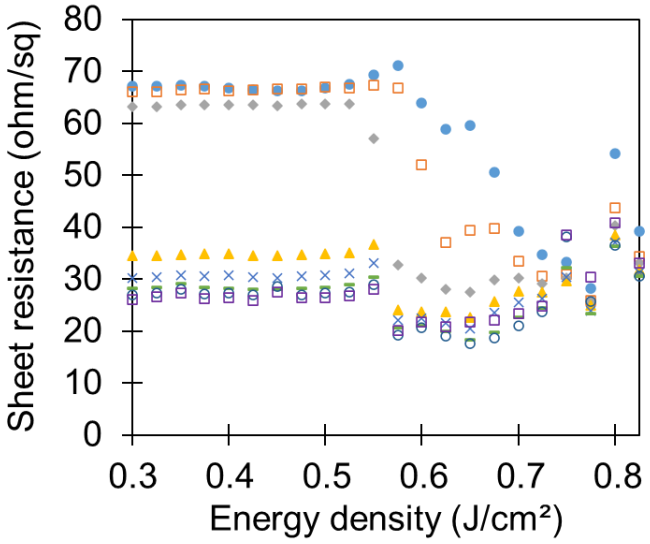
Sheet resistance (ohm/sq)
80
70
60
50
40
30
20
10
0
0.3
0.4
0.5
0.6
0.7
0.8
Energy density (J/cm²)

a)

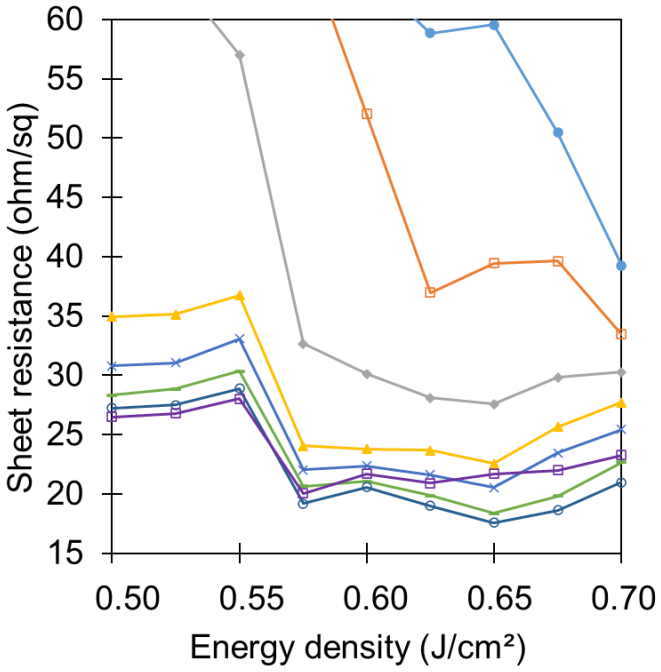
Sheet resistance (ohm/sq)
60
55
50
45
40
35
30
25
20
15
0.50
0.55
0.60
0.65
0.70
Energy density (J/cm²)

b)

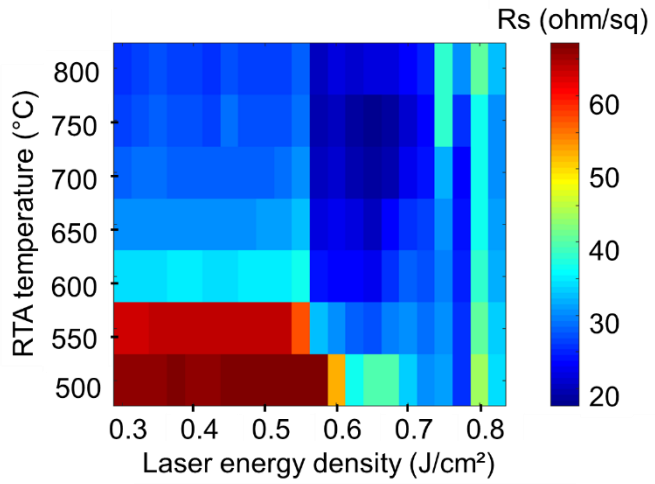

c)

Figure 5 *: Sheet resistance as a function of the laser energy density between 0.300 J/cm² and 0.825 J/cm² (0.025 J/cm² steps) for TiN 15 nm / a-Si 10 nm / Ti 10 nm / a-Si 10 nm / c-Si (substrate) multilayer samples submitted to 3 UV-NLA pulses and c-RTA at temperatures between 500 and 800 °C (and with no RTA). a) Evolution over the full range (graph with markers). b) Zoom (lines and markers) on the Rs decrease between 0.500 and 0.700 J/cm². c) 2D color map. Each rectangle corresponds to a given energy density as well as a given temperature and its color corresponds to the sheet resistance value.*

Figure 5 shows Rs measurements for multilayer samples, i.e. TiN 15 nm / a-Si 10 nm / Ti 10 nm / a-Si 10 nm / (100) Si stacks after 3 UV-NLA pulses and after each cumulative RTA (similarly to results presented in Fig. 3). After 3 UV-NLA pulses without any RTA, Rs is stable around 65 Ω/sq for EDs lower than 0.525 J/cm² (blue circles). Between 0.525 J/cm² and 0.575 J/cm², Rs increases, reaching a maximum of 71 Ω/sq. Between 0.600 J/cm² and 0.775 J/cm², Rs decreases down to approximately 30 Ω/sq. Then, for EDs higher than 0.775 J/cm², Rs increases again.

When a subsequent c-RTA is applied at 500 °C or up to 550 °C, Rs remains stable around 65 Ω/sq for low UV-NLA energy densities (orange squares and grey diamonds). For c-RTA up to temperatures between 600 and 800 °C (yellow triangles, blue crosses, green dashes, unfilled blue circles and unfilled purple squares) Rs exhibits a plateau for low ED but at a lower value, around 30 Ω/sq. Rs decreases at 0.575 J/cm² then reaches a plateau around 20 Ω/sq up to 0.725 J/cm² as seen on Figure 5b. For EDs 0.750 J/cm² and higher, Rs is higher.

Figure 5c further evidences: (i) the sharp Rs decrease in the 0.575 - 0.625 J/cm² range for c-RTA temperatures between 550 and 600 °C, and, (ii) the low Rs valley in the 0.575 - 0.750 J/cm² range for c-RTA temperatures from 550 up to 800 °C. Figure 6 shows XRD measurements corresponding to multilayer samples after UV-NLA and a subsequent c-RTA up to 800 °C.

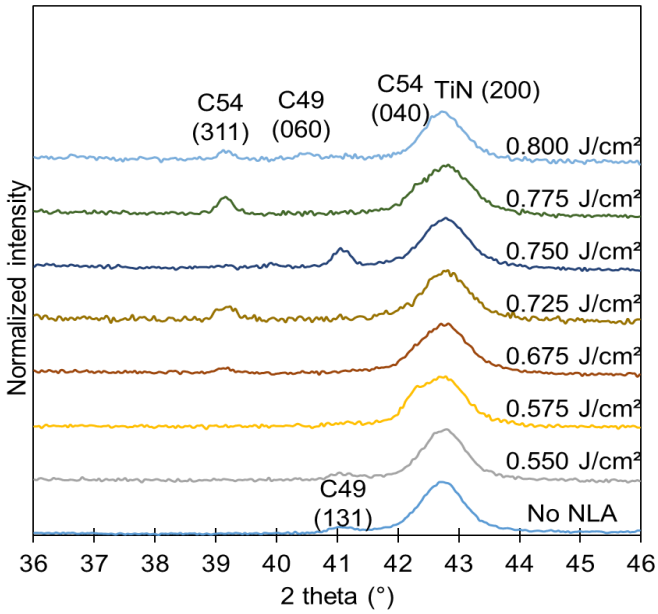

a)

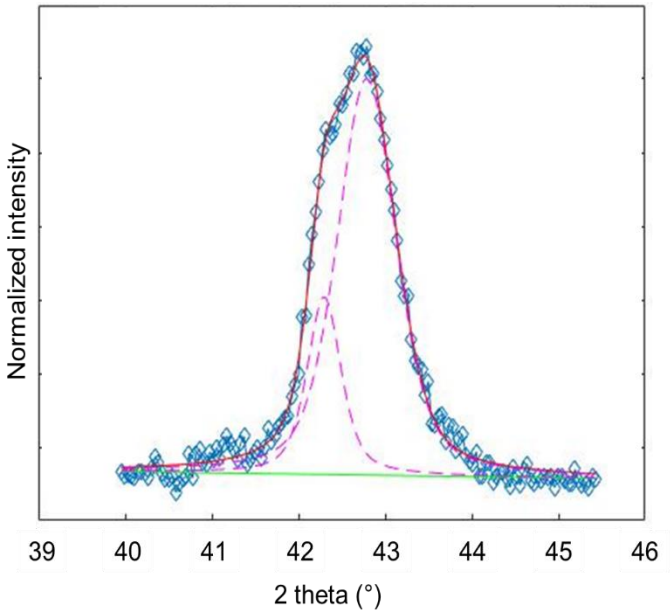

b)

Figure 6 *: XRD profiles for TiN 15 nm / a-Si 10 nm / Ti 10 nm / a-Si 10 nm / c-Si multilayer samples after 3 UV-NLA pulses (ED between 0.550 J/cm² and 0.800 J/cm²) then c-RTA up to 800 °C. XRD data for a similar sample without UV-NLA treatment ('No NLA') but still with c-RTA up to 800 °C is shown for comparison. b) Deconvolution of the 2 peaks seen between 42 ° and 43 ° approximately, for a multilayer sample after 3 UV-NLA pulses (ED: 0.575 J/cm²) and a c-RTA up to 800 °C.*

In all multilayer samples, the capping layer is evidenced by a TiN (200) peak at 42.7 ° and not the TiN (111) peak at 36.7 ° that was observed for reference samples. There is thus a change in texture between the reference TiN / Ti / c-Si samples and multilayer samples.

It is certainly due to the different layer on which TiN has been deposited: for the multilayer stack, TiN has been deposited on an amorphous Si layer, resulting in a (200) orientation. Meanwhile, for the reference sample, it has been deposited on Ti (crystalline), resulting in a (111) orientation. This change of texture could potentially change the surface roughness, modifying laser absorption. However, this was not observed (at least within measurement uncertainties). Moreover, a check of the roughness of the TiN surface layer using Atomic Force Microscopy (AFM) was performed on as-deposited samples, without any UV-NLA or RTA (not shown). The surface root mean square roughness of the two samples were similar: 0.39 nm for the reference sample and 0.31 nm for the multilayer stack. It was thus likely that laser absorption was not impacted by the different textures of TiN.

For samples submitted to c-RTA up to 800 °C without UV-NLA beforehand, and for low energy density NLA (0.550 J/cm² or less), the C49-$TiSi_2$ phase was the only silicide phase detected with a (131) peak at 41.1 °. For ED values between 0.575 J/cm² and 0.650 J/cm², there was a shoulder at low angle (around 42.2 °) close to the TiN peak that could be attributed to the C54-$TiSi_2$ (040) peak. The two peaks in this shoulder are deconvoluted in Fig. 6b. Between 0.675 J/cm² and 0.725 J/cm², the C54-$TiSi_2$ (311) peak at 39.1 ° was also detected. It was also present at 0.775 J/cm². For 0.750 J/cm², only the C49-$TiSi_2$ was evidenced. Then, for an ED of 0.800 J/cm², there was a mix of C49-$TiSi_2$ and C54-$TiSi_2$ phases.

4 Discussion

4.1 Formation of the aimed microstructure

Figure 7 is a schematic of the phases in presence, and microstructure, after UV-NLA and c-RTA obtained for the reference samples (Fig. 7a and 7b) and multilayers (Fig 7c and 7d) as a function of the UV-NLA energy density. In Figs. 7b and 7d, the lowest temperature yielding the C54-$TiSi_2$ phase has been selected for c-RTA, i.e. 650 °C for the reference samples (Fig. 7b) and 600 °C for multilayers (Fig. 7d).

The understanding of the phase sequence and microstructure of each phase is key to promote C54-$TiSi_2$ phase formation. In this work, the microstructure obtained after UV-NLA for conditions enabling the subsequent formation of the C54-$TiSi_2$ phase (only) by c-RTA, has been assumed to be a matrix of amorphous silicide with grains of C40-$TiSi_2$ as suggested by Esposito et al [42]. Such matrix has not been directly observed but it is a reasonable possibility based on the Rs decrease for the corresponding process conditions., which is a matrix of amorphous silicide with grains of C40-$TiSi_2$ phase, has not been directly observed. It is a possibility that is based on the decrease of

Rs values. The hypothetical nature of this microstructure will not be systematically recalled in this paper.

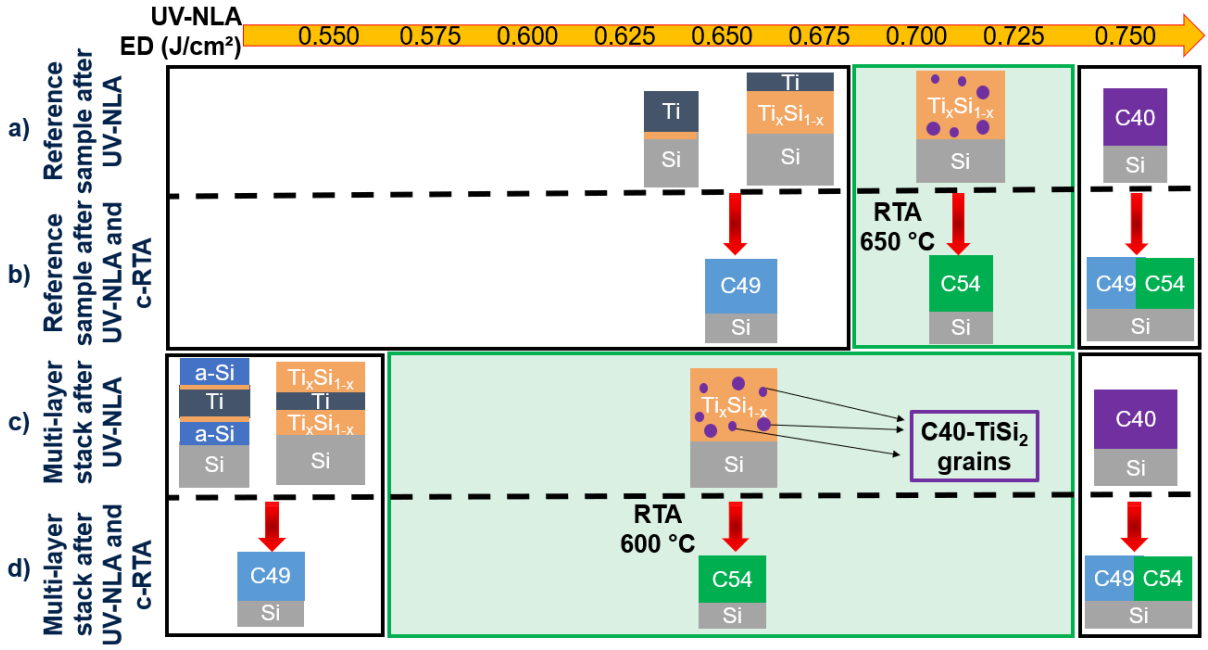

Figure 7 *: Summary of C54-$TiSi_2$ phase sequence formation using a) UV-NLA for the reference samples b) UV-NLA and c-RTA up to 650 °C for the reference samples c) UV-NLA for multilayers d) UV-NLA and c-RTA up to 600 °C for multilayers. For the sake of clarity, the TiN capping layer is not represented as it is not supposed to take part in the reactions.*

After laser annealing, the global behavior and the phase sequence are similar for reference samples and multilayers, even if the UV-NLA energy density and the c-RTA temperature corresponding to different stages may differ. In a previous work, we already detailed the early stages of silicidation upon UV-NLA [43]. At low ED, Si atoms diffuse to form an amorphous silicide labelled Ti_xSi_{1-x}, resulting in a slight Rs increase after the first plateau (See 'No RTA' samples in Fig. 3 for ED ~0.625-0.675 J/cm² and Fig. 5 for ED ~0.525-0.575 J/cm²). For intermediate ED, the Rs decrease in Fig. 3 and 5 is likely due to the appearance of a matrix of amorphous silicide with C40-$TiSi_2$ grains. Indeed, in these samples the partial formation of the C40-$TiSi_2$ phase reduces the sheet resistance. Esposito et al. have shown by TEM on similar samples the coexistence of the amorphous silicide and the C40-$TiSi_2$ phase [42-44]. An explanation of this Rs decrease (Fig. 5) could be found considering the percolations paths between the C40-$TiSi_2$ grains. Those percolations paths have not been observed by TEM because of a lack of contrast and resolution for those measurements, yet they may still be present in multilayer samples. When the percolation threshold is reached, a path is formed between two isolated grains. Then, the more grains nucleate, the more percolation paths are obtained, and the more resistivity of the sample decreases [45]. For higher EDs, only the C40-$TiSi_2$ phase is obtained.

Figure 7 shows that the phases obtained by c-RTA are closely related to the phases and microstructures obtained after UV-NLA. Indeed, for low ED and c-RTA, the microstructure after UV-NLA is similar to the one after deposition and the phase is similar to the one obtained when only the RTA is applied, and thus there is no clear impact of UV-NLA. In this case, only the C49-$TiSi_2$ phase is formed, for c-RTA at a temperature lower than 700 °C. For intermediate ED and c-RTA, the microstructure made of amorphous silicide and grains of C40-$TiSi_2$ is obtained after UV-NLA and the C54-$TiSi_2$ phase is formed alone at low RTA temperatures, as required for optimized contacts.

For high ED and c-RTA, only the C40-$TiSi_2$ phase is observed after UV-NLA and a mix of C49-$TiSi_2$ and C54-$TiSi_2$ is obtained after RTA, as evidenced by the final Rs increase in Fig. 5. Yet, the size and the phase proportions for the mixture of C49-$TiSi_2$ and C54-$TiSi_2$ phases obtained after NLA with a high ED and subsequent c-RTA up to 800 °C have not been investigated in detail. So, the schematic representation of the microstructure of this mixture in the Figure 7b (for high ED) is not quantitively representative of the actual microstructure after these heat treatments.

An important difference between reference samples and multilayers lies in the ED values for which the phase sequence takes place, and in particular the possibility to form the C54-$TiSi_2$ phase alone after a low thermal budget RTA: a single one (0.700 J/cm²) for reference samples and a range of lower ED (0.575-0.650 J/cm²) for multilayers. This extended range of low ED values for multilayers is interesting for a technologically relevant salicide process as the process window is wider. Figure 8 is a schematic showing the possible evolution of the microstructure before, during and after laser annealing with optimal ED conditions for the future formation of the C54-$TiSi_2$ phase during a subsequent RTA at low temperatures.

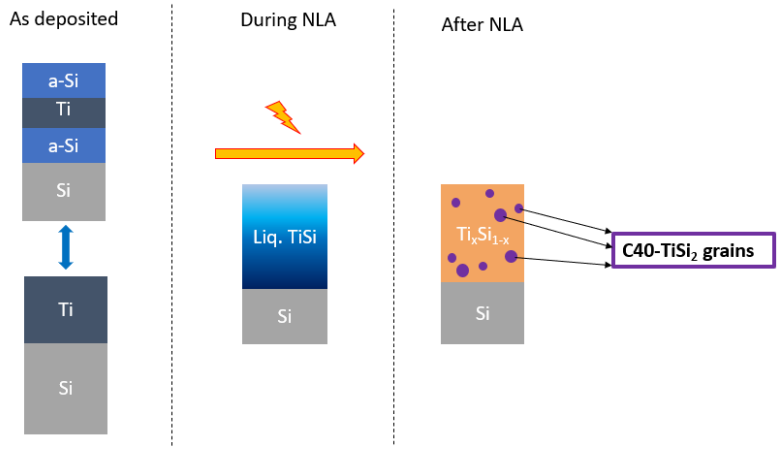

Figure 8 *: Diagram of the formation of the microstructure of interest upon UV-NLA.*

Esposito et al. [42-43] have explained that the nucleation of the C54-$TiSi_2$ phase during a RTA was more likely to happen with the favorable microstructure [43] obtained after UV-NLA consisting in a matrix of amorphous silicide with grains of C40-$TiSi_2$ grains. This microstructure

should result from the liquid phase upon cooling after UV-NLA. Indeed, during the laser pulse, a liquid silicide phase is formed because of the melting of Si The Si should start to melt first and the liquid could then consume the Ti layer and/or the amorphous silicide to form a liquid phase containing both Si and Ti. As the melting temperature of a-Si is lower than the one of c-Si, the liquid phase is thus likely to be influenced mainly by the a-Si layers. Therefore, using a-Si enables to get a liquid phase for an ED relatively low during laser annealing, resulting in the entire consumption of Ti. Then, during the cooling, some grains of C40-$TiSi_2$ nucleate and the remaining liquid transforms into an amorphous silicide matrix. For higher ED, a few nanometers of monocrystalline Si from the substrate could also melt.

This favorable microstructure described in Fig. 8 can promote the formation of the C54-$TiSi_2$ phase at lower RTA temperature because the nucleation barrier for C54-$TiSi_2$ phase formation is lower at the amorphous silicide / C40-$TiSi_2$ phase interface than in the bulk of the C40-$TiSi_2$ phase and even more than in the bulk of the C49-$TiSi_2$ phase. The main parameters of this low nucleation barrier are the high driving force at the amorphous silicide / C40-$TiSi_2$ phase interface and the low energy of the C54-$TiSi_2$ phase / C40-$TiSi_2$ phase [42-43].

For high ED and c-RTA, a mix of C49-$TiSi_2$ and C54-$TiSi_2$ phases is formed. The formation of this mix could be due to the amount of molten c-Si during the UV-NLA, which could lead, after cooling, to the full formation of C40-$TiSi_2$ after UV-NLA and finally, to the formation of a large amount of C49-$TiSi_2$ with C54-$TiSi_2$ grains after RTA.

To summarize, nanosecond laser annealing with appropriate energy densities can result in a matrix made of amorphous silicide with C40-$TiSi_2$ grains that promote the formation of the C54-$TiSi_2$ phase upon a subsequent RTA at moderate temperature. Similarities and differences between reference samples and multilayers will now be discussed.

4.2 Phase formation by UV-NLA

For reference samples and multilayers submitted to NLA only, Rs measurements show the same global behavior: there is a plateau for low ED, followed by a slight increase, and finally a decrease with eventually another rise for the highest ED. The plateau at low ED can be explained by considering that the ED is too low to induce any stack change. The slight increase at intermediate ED is due to the formation of an amorphous silicide [43]. Meanwhile, the final rise is due to the formation of several $TiSi_2$ phases which could have higher resistivity.

Even if the global behavior is the same, Figure 9 shows that there are differences between Rs values for the reference samples and multilayers. Indeed, the way Rs decreases and the ED at which this decrease starts change between both types of samples.

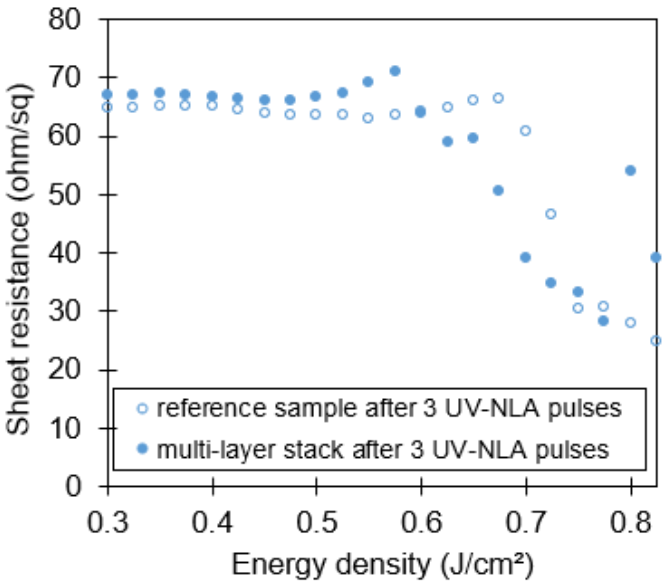

Figure 9 *: Rs evolution as a function of the laser ED for multilayers and reference samples after 3 UV-NLA pulses.*

As far as reference samples are concerned, the Rs decrease is sharp, continuous and starts at 0.700 J/cm². As explained before, this decrease is linked to the formation of the C40-$TiSi_2$ phase through Si melting (Fig. 8). Note that neither C40-$TiSi_2$ nor any other silicide phase was observed by XRD after UV-NLA in the range corresponding to this Rs drop (not shown) but this is certainly because the volume of crystalline silicide is too low to be detected by XRD.

For multilayers, the decrease starts at 0.600 J/cm². Moreover, Rs does not continuously decrease as there is a step between 0.600 and 0.650 J/cm². This plateau is likely due to the consumption of all the amorphous silicon: there is no more a-Si available to form more C40-$TiSi_2$ and Rs remains steady at 60 Ω/sq. For higher ED, crystalline Si starts to melt and the decrease continues monotonously to reach a value of about 30 Ω/sq for 0.775 J/cm². For the reference sample, this value of 30 Ω/sq is also reached for the same ED but Rs continues to slightly decrease for higher ED. These results show that the microstructure of interest should be obtained for a lower ED and with a wider process window using a-Si layers.

To have a better understanding of the difference between reference samples and multilayers, the temperatures reached during UV-NLA were simulated with the LIAB software (LASSE Innovation Application Booster). Simulations were carried out in one dimension (perpendicular to the surface), by solving the heat equation coupled to the time-harmonic solution of Maxwell equations [46-48]. The calculated surface temperatures in multilayers during a UV-NLA pulse are shown in Figure 10 for different EDs (between 0.600 J/cm² and 0.775 J/cm² with a step of 0.025 J/cm²). As discussed before, the formation of the C40-$TiSi_2$ phase requires to go through

a liquid phase. **Table 1** summarizes the melting point temperatures of the different materials used for simulation.

Table 1 : Melting temperatures of different materials present in the studied samples and taking part to the titanium silicidation.

Phase	**c-Si**	**a-Si**	**Ti**
Melting point (°C)	**1415 [2]**	**1150 [47]**	**1668 [2]**

As far as multilayers are concerned, the liquid phase should be first formed by melting amorphous silicon as it has a lower melting point than c-Si (Table 1). Moreover, the liquid phase could possibly contain some molten amorphous Ti_xSi_{1-x} because its melting temperature should be relatively similar to the a-Si phase. The Ti_xSi_{1-x} amorphous phase could form during the deposition of the Ti layer [42] and/or during annealing [42]. However, due to the very low deposition temperature (70 °C), the thickness of intermixing layer present prior to any laser pulse should be around 1 or 2 nm. Therefore, the amount of molten amorphous Ti_xSi_{1-x} should be negligible for the LIAB simulations. The simulated temperature corresponds to the surface temperature, which is the TiN surface layer temperature in this case. The surface temperature is equivalent to the temperature in the full depth of multilayers thanks to the good thermal conductivity of Si, Ti, and TiN. Indeed, the top surface should be only 1 % higher compared to the bottom of the stack. In Fig. 10, for all ED, the top surface temperature reaches a maximum for a time around 190 ns, then starts the cooling. For 0.625 J/cm², a plateau is reached, corresponding to the melting temperature of the a-Si layer which is around 1150 °C [47]. For 0.725 J/cm², another plateau is reached, corresponding to the melt onset of c-Si from the substrate (maximum temperature simulated for an ED of 0.725 J/cm²: 1445 °C).

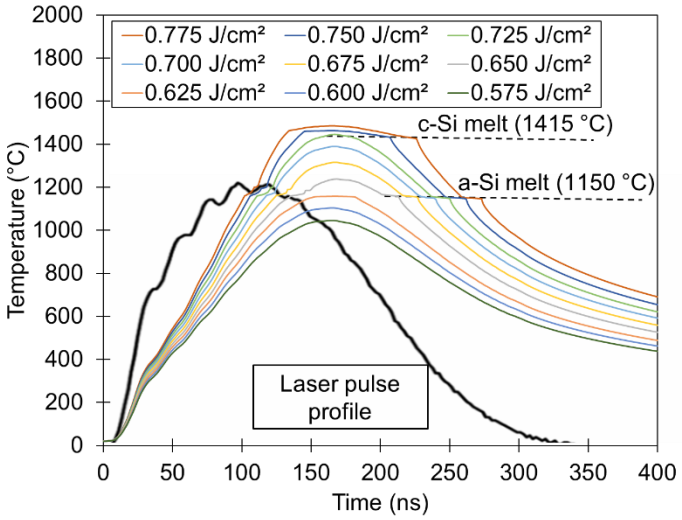

Figure 10 *: Simulated surface temperature as a function of time during a UV-NLA pulse on a multilayer stack TiN 15 nm / a-Si 10 nm / Ti 10 nm / a-Si 10 nm / c-Si (substrate). The laser intensity is also plotted as a function of time (black curve).*

The switch to the liquid state estimated by the LIAB simulations was confirmed by in-situ reflectivity (TRR) measurements during each UV-NLA pulse. Color maps of the in-situ reflectivity as a function of ED and time during the first UV-NLA pulse are shown in Figures 11a and 11b for the reference and multilayer samples.

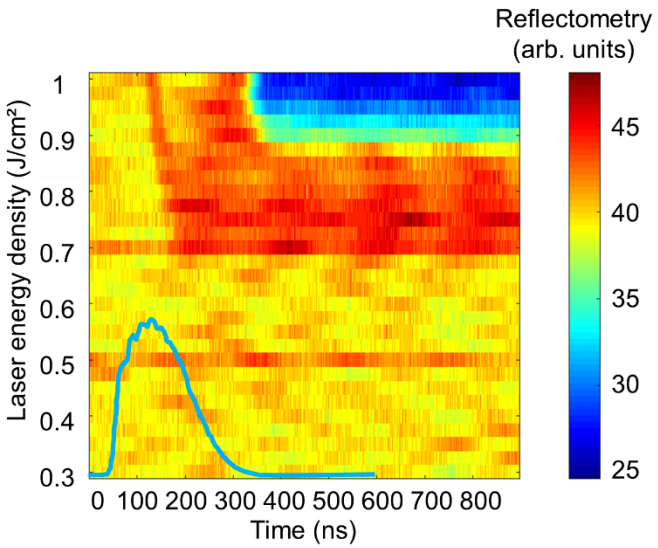

a)

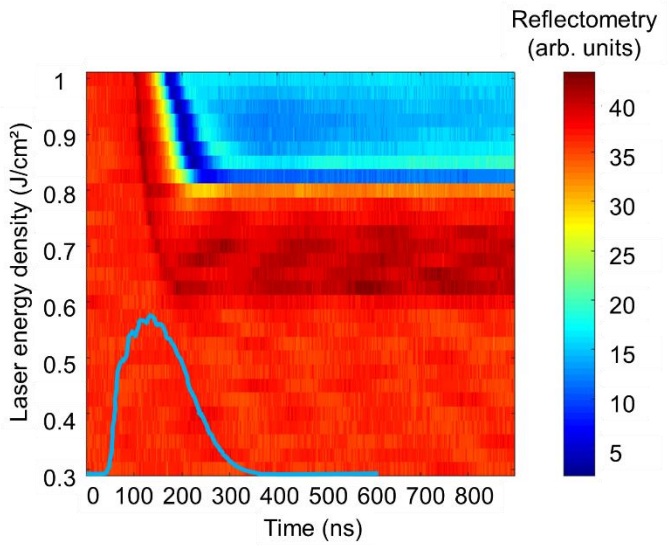

b)

Figure 11 *: Color maps of in-situ surface reflectivity as a function of time and ED during the first laser pulse for a) TiN 15 nm / Ti 10 nm / c-Si (substrate) reference samples, and b) for TiN 15 nm / a-Si 10 nm / Ti 10 nm / a-Si 10 nm / c-Si (substrate) multilayers. The laser intensity is also plotted as a function of time (blue curve).*

The blue line included in both Fig. 11a and 11b represents the laser pulse. For reference samples (Fig. 11a), the surface reflectivity is stable at low ED. It increases for ED 0.700 J/cm² and above. A similar observation can be made for multilayers (Fig. 11b) but at a lower ED value, close to 0.600 J/cm². Such reflectivity change is very likely due to the melting of some material below the TiN cap. Indeed, the melting of a material such as bulk Si, usually leads to an abrupt reflectivity increase [49]. In our case, the top TiN layer and the initial thicknesses of the different layers make the observation more complex. However, we still can evidence the transient presence of a liquid phase containing Si and Ti, from 0.600 and 0.700 J/cm² for multilayers and reference samples, respectively. Thus, thanks to the presence of a-Si layers, multilayers would enable the transient formation of a liquid TiSi phase at lower ED values than reference structures. As for reference samples, the transient liquid phase is needed to reach the microstructure made of a matrix of amorphous silicide with C40-$TiSi_2$ grains [42-44] after cooling. Yet, there is an ED shift for the formation of the liquid phase between reference samples and multilayers. This shift corresponds to the shift in the decrease of Rs values (Figs. 3 and 5) and is due to the lower melting temperature of a-Si compared to c-Si (Table 1). Consequently, after cooling, the microstructure made of a matrix of amorphous silicide with grains of C40-$TiSi_2$ would be obtained at lower ED in multilayers. To further confirm the presence of a transient liquid phase, top-view SEM observations were performed on the reference samples (Figure 12a) and on multilayers (Figure 12b).

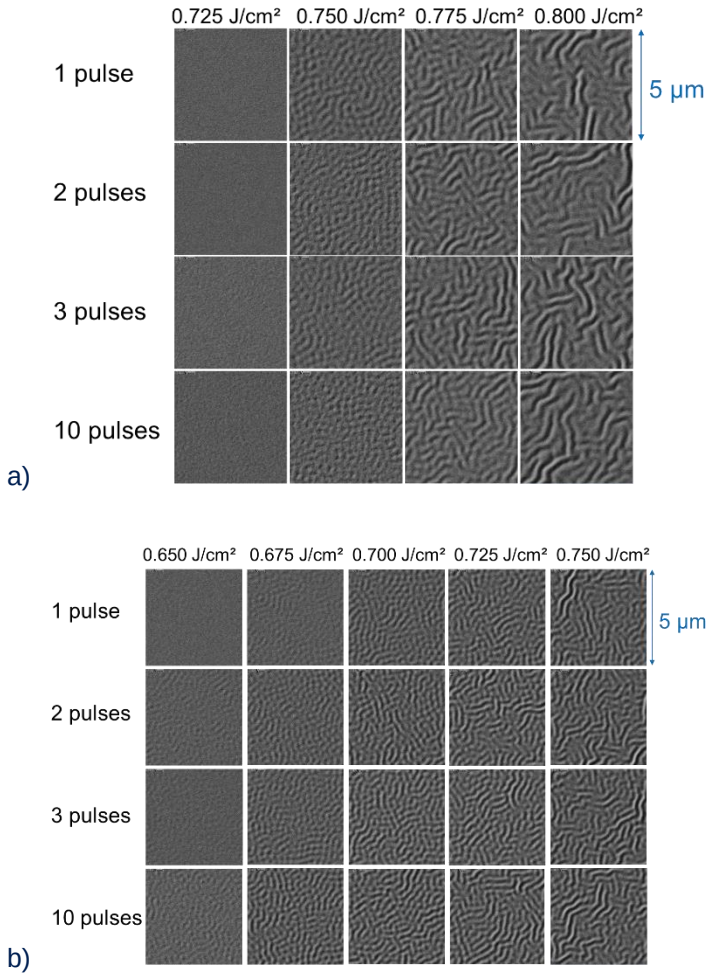

Figure 12 *: Top-view 5×5µm² SEM images after 1, 2, 3 and 10 laser pulses for a) TiN 15 nm / Ti 10 nm / c-Si substrate reference samples, and b) TiN 15 nm / a-Si 10 nm / Ti 10 nm / a-Si 10 nm / c-Si substrate multilayers at various laser energy densities (on top).*

After 1, 2, 3 or 10 UV-NLA pulses, some wrinkles appear for ED = 0.650 J/cm² and above for multilayers. Meanwhile, they appear at ED = 0.750 J/cm² and above for reference samples. Given that the TiN top layer is solid and the substrate rigid, it is necessary to have at least 20 nm of a liquid phase in between TiN and the substrate to observe surface ripples after cooling [50]. In our specific case, ripples result from the relaxation of the compressive TiN cap temporarily lying on a liquid layer. Therefore, the appearance of ripples is a good indicator of the formation of the liquid phase, but the essential ED value is the one corresponding to the increase of the in-situ reflectivity, i.e. 0.600 J/cm² after 1 UV-NLA pulse for multilayers. Indeed, a liquid phase is needed to form the desired microstructure, and this formation can start even with a thin liquid phase (less than 20 nm). Therefore, it clearly shows that a liquid phase is obtained during laser annealing, but the ED corresponding is overestimated by SEM observations compared to TRR (Fig. 11), and Rs measurements (Fig. 5), due to the minimum of 20 nm of liquid needed to observe ripples. The

melting of a-Si layers, predicted by the 1D numerical simulations, is evidenced by TRR and the SEM observations. It is expected to lead to the desired microstructure, as shown by decreasing Rs values. Therefore, Rs, in situ reflectivity and SEM as well as simulations all show that the use of a-Si layers enables to reduce the ED needed to obtain a liquid phase, and, by extension, the favorable microstructure.

Although no crystalline silicide phase was identified by XRD right after 3 UV-NLA pulses at 0.650 J/cm² (not shown), the Rs decrease shown in Fig. 5 can only be explained by the presence of some grains with a $TiSi_2$ phase as the $TiSi_2$ phase has a relatively low resistivity. This crystalline $TiSi_2$ phase could be the C40-$TiSi_2$ phase, the C49-$TiSi_2$ phase or the C54-$TiSi_2$ phase. However, it has been shown that the silicide phase that is usually formed after UV-NLA, is the C40-$TiSi_2$ phase [40, 42]. Based on the work of Esposito et al. [42], for this thermal treatment, this silicide layer might correspond to a mixture of amorphous silicide with C40-$TiSi_2$ grains. The presence of such a mixture is investigated by TEM-EDX measurements shown in Figure 13.

Fig. 13 shows a cross-sectional TEM image and the corresponding EDX profiles of a multilayer (TiN 15 nm capping layer / a-Si 10 nm / Ti 10 nm / a-Si 10 nm / c-Si substrate) after 3 UV-NLA pulses at 0.650 J/cm². This sample has been specifically selected because the most favorable microstructure should be formed. The EDX profile in Fig. 13b shows that a large amount of carbon is present, particularly in the Pt protection layer used for the sample preparation. Consequently, this C contamination induces an uncertainty on the atomic percentages of other species. However, the concentration ratio, Si/(Si+Ti), in the silicide layer is close to 0.6. This ratio is lower than 2/3 expected for $TiSi_2$ and is in line with a mixture of amorphous silicide and C40-$TiSi_2$.

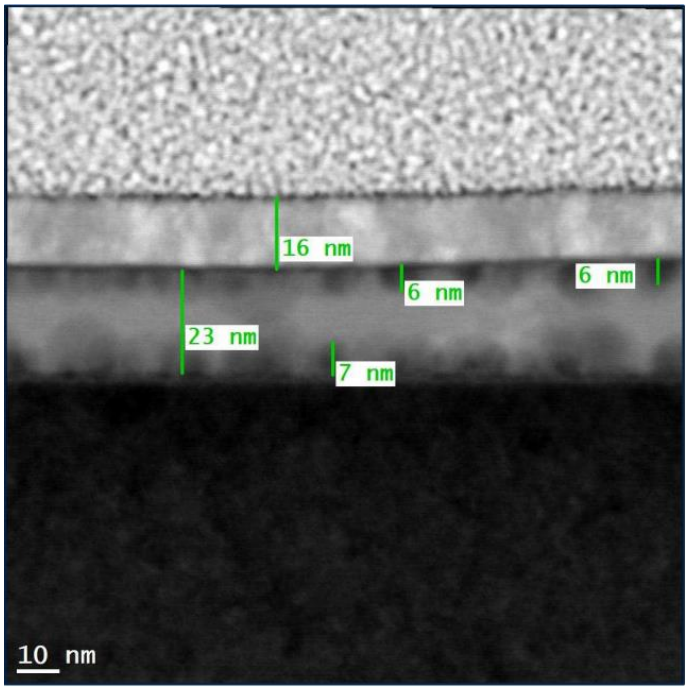

a)

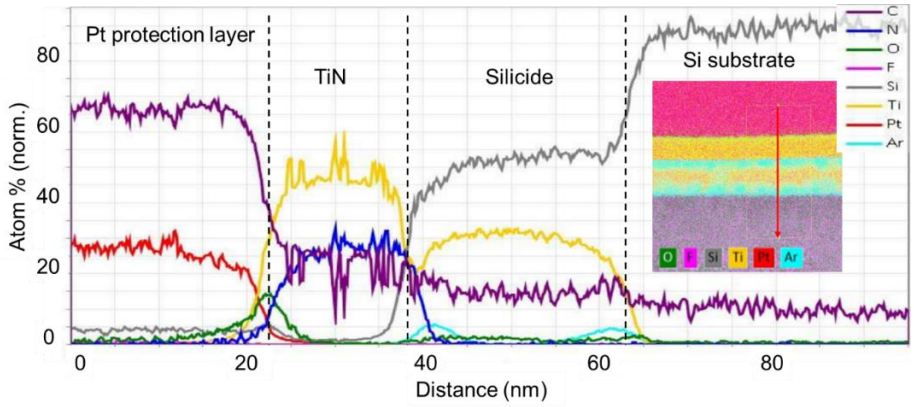

b)

Figure 13 *: Cross-sectional TEM on a (TiN 15 nm / a-Si 10 nm / Ti 10 nm / a-Si 10 nm / c-Si substrate) multilayer after 3 UV-NLA pulses at 0.65 J/cm²: (a) TEM image (b) EDX depth profiles along the line drawn in the insert showing the EDX map of a).*

Figure 13a shows that the silicide film has a thickness of 23 nm. Starting from 10 nm of Ti, it could be possible to obtain 25 nm of $TiSi_2$ by consuming 23 nm of Si [42]: thus, the silicide film thickness is slightly too low. Moreover, there are some cavities, appearing as dark and round zones, near the TiN / silicide and silicide / c-Si interfaces. These pores are located at the initial location of the a-Si layers and their size (6-7 nm) represents a large part of the initial a-Si thickness (10 nm).

The silicide thickness and the presence of cavities shows that the amount of deposited a-Si has been over evaluated. The pores observed by TEM might result from the PVD deposited Si films that can be porous. As the a-Si films had a total nominal thickness of 20 nm and were likely porous, the amount of Si was not enough to form a silicide film with a $TiSi_2$ stoichiometry. Since

the decrease of Rs values (Fig. 5) shows the formation of a $TiSi_2$ phase, the silicide film should be a mixture of a $TiSi_2$ phase and another phase with a composition poorer in Si, such as amorphous Ti_xSi_{1-x}. However, the grains may be too small to be observed by TEM or XRD. It certainly corresponds to the microstructure described by Esposito et al. [42-43] which is a matrix of amorphous silicide with C40-$TiSi_2$ grains.

The EDX profiles and maps in Fig. 13b show that the pores at the TiN/silicide and silicide/substrate interfaces are filled with Ar. Those cavities are probably due to the PVD deposition that was performed with an Ar-based plasma. This technique is known to produce porous deposited layers and the Ar-based plasma PVD is the only source of argon during the production of multilayers. Moreover, these pores could possibly be enlarged by a Kirkendall effect [51] during UV-NLA: the Ar/silicide interfaces could move by diffusion and small pores could grow by coalescence. In addition, the Ga beam of the FIB could enlarge pores during TEM sample preparation.

As shown in the schematic of Fig.7, they are two main differences between reference samples and multilayers: (i) the minimum ED needed to obtain the targeted microstructure (i.e. an amorphous Ti_xSi_{1-x} matrix containing C40-$TiSi_2$ grains) is lower for multilayers (ii) there is a much larger range of ED yielding the targeted microstructure for multilayers. As detailed previously, the lower ED threshold is due to the lower melting point of a-Si. The microstructure is also obtained because (i) only a-Si melts and (ii) the amount of a-Si is not large enough to fully convert the Ti film into $TiSi_2$. The melting of the a-Si layers will thus result in the targeted microstructure as long as c-Si does not melt. Indeed, when c-Si melts, Ti can be fully converted into C40-$TiSi_2$ and not anymore in the targeted microstructure. Simulations (Fig. 10) show that melting occurs at 0.625 and 0.725 J/cm² for a-Si and c-Si, respectively. The targeted microstructure should thus be present between these two ED. This is in qualitative agreement with Rs measurements (see Fig. 5, 'No RTA' sample) but simulations seem to overestimate the ED needed for melting since the experiment ED range is found between 0.575 and 0.650 J/cm² for 3 pulses. This might be due to the 3 pulses since simulations were performed for a single pulse. Reactions and/or intermixing occurring before melting may also change the melting point. Whatsoever the use of a-Si layers with limited thickness enables to lower the required ED and widen the ED range of interest. The process window is thus enlarged as it starts with a-Si melting and ends with c-Si melting: it corresponds to the formation of a microstructure made of an amorphous silicide matrix with C40-$TiSi_2$ grains.

4.3 After UV-NLA and a subsequent cumulative RTA

Figure 14 focuses on the sheet resistance of both types of samples after 3 UV-NLA pulses with a subsequent c-RTA up to 600 °C for multilayers and 650 °C for the reference samples. These two temperatures (650 °C for the reference samples and 600 °C for multilayers) were selected as they corresponded to the minimum temperature for which Rs was the lowest for both types of samples. Indeed, for reference samples, a c-RTA up to 650 °C resulted in low Rs for ED between 0.675 and 0.725 J/cm², with a minimum for the latter (Fig. 14). This minimum around 10 Ω/sq corresponded

to the formation of C54-$TiSi_2$ as the only silicide (Fig. 4). For a c-RTA up to 600 °C, there was an increase at ED = 0.650 - 0.675 J/cm² and the R_S minimum was not as low, for reference samples, than at 650°C (hence the choice of the latter). This Rs around 10 Ω/sq after UV-NLA than c-RTA up to 650 °C was actually similar to Rs values obtained after c-RTA only up to 800 °C.

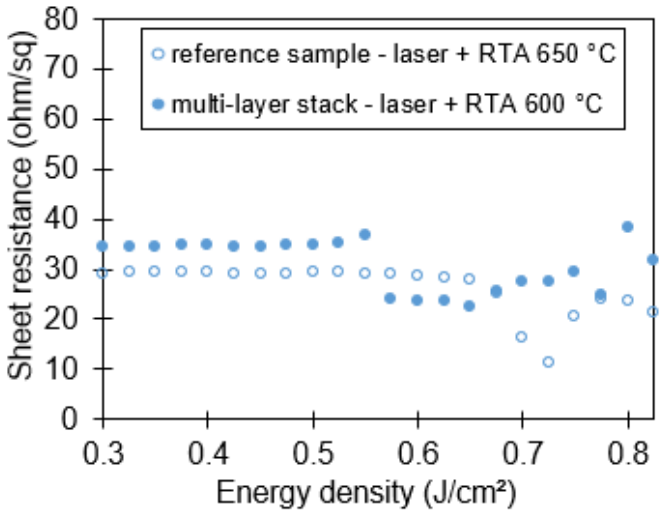

Figure 14 *: Sheet resistance as a function of the laser energy density after 3 UV-NLA pulses then some c-RTA for two sets of samples: multilayers with a c-RTA up to 600 °C and reference samples with a c-RTA up to 650 °C.*

Meanwhile, for multilayers, a c-RTA up to 600 °C or more leads to a Rs decrease for ED between 0.575 J/cm² and 0.650 J/cm² (Fig. 14). It is associated with the formation of C54-$TiSi_2$ as the main silicide phase (Fig. 6). For a c-RTA up to 550 °C, Rs values were close to that at 600°C, e.g. close to 25 Ω/sq, but still not as low.

XRD measurements (Fig. 4 and 6) showed that, for reference samples and multilayers, only the C54-$TiSi_2$ phase was obtained when Rs was the lowest. XRD measurements were performed after c-RTA up to 800 °C but given the similar Rs values, the C54-$TiSi_2$ phase should be also present after c-RTA up to 600 °C. The value of 10 Ω/sq for reference samples also corresponds to the resistivity of the C54-$TiSi_2$ phase if one considers that the whole 10 nm Ti layer has been consumed, resulting in a theoretical silicide thickness of 25 nm.

In order to understand Rs minimum differences between the two types of samples, TEM analysis was performed on a multilayer after a c-RTA up to 800 °C with no UV-NLA (Figure 15). Fig. 15a shows a cross-sectional TEM image, with the location where EDX measurements were performed, and Figure 15b shows the corresponding EDX profiles.

a)

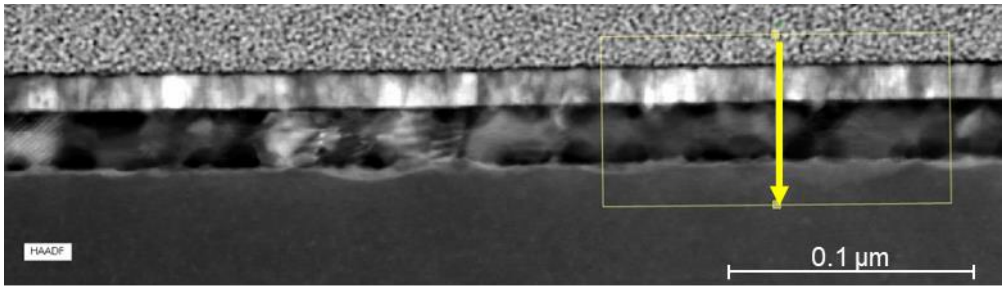

b)

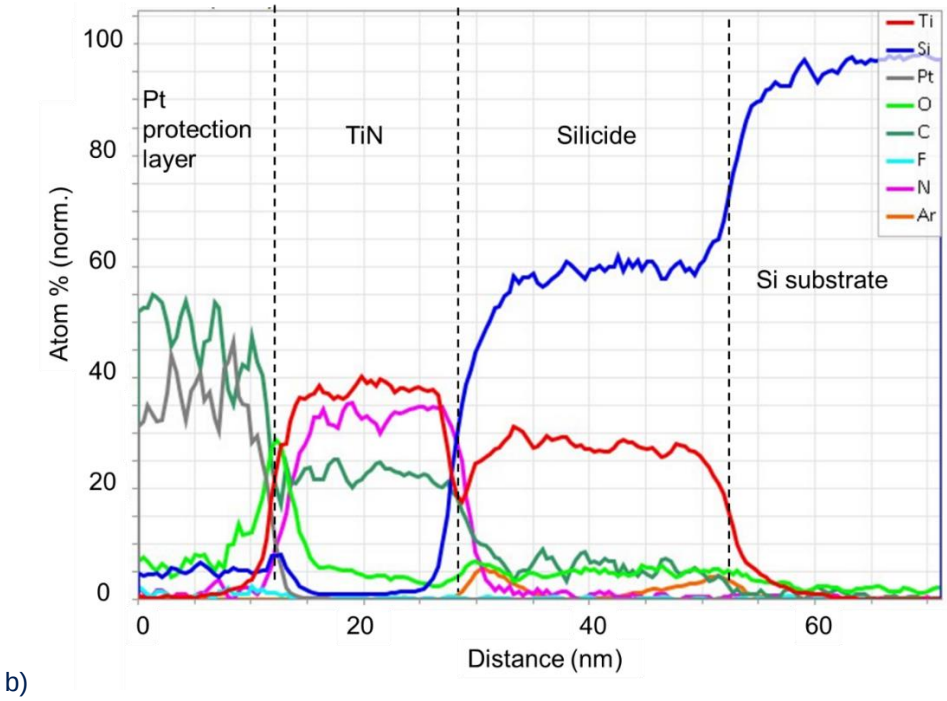

Figure 15 *a) cross-sectional TEM image of a multilayer on which EDX depth profiles were extracted along the yellow arrow. This sample was observed after a c-RTA up to 800 °C only (no UV-NLA). b) Corresponding EDX depth profiles.*

The silicide layer thickness is close to 21 nm. The TiN layer is C-rich and there is some slight oxidation at the TiN/silicide interface, with approximately 5% of O in the silicide. The C49-$TiSi_2$ phase identified by XRD (Fig. 6) for this sample is consistent with the Ti and Si atomic contents found in the silicide layer. Pores are also visible (Fig. 15a) for this sample after c-RTA up to 800 °C. This indicates that pores already observed after UV-NLA (Fig.13) are also present after solely a c-RTA up to 800 °C. Based on these observations, similar pores are also expected for samples submitted to both UV-NLA and c-RTA. EDX profiles evidence the presence of Ar at the TiN/$TiSi_2$ and $TiSi_2$/Si interfaces. The presence of these Ar filled pores may explain why the Rs minimum is about 25 Ω/sq for multilayers, e.g. roughly two times that of reference samples (10 Ω/sq). This Rs value for the reference sample corresponds to a layer fully made of C54-$TiSi_2$. The presence of pores decreases the effective silicide thickness through which electrons need to pass through, leading to a higher sheet resistance. Pores could also have increased the surface and the interface

of the silicide film that could also contribute to the increase in Rs. Nevertheless, multilayers enables to obtain low resistivity C54-$TiSi_2$ with a wider ED process window, an ED lowered by 0.100 J/cm² and with an RTA temperature 50°C lower than for reference samples.

The transient microstructure with a favorable proportion of amorphous silicide and C40-$TiSi_2$ grains appears to be quite sensitive to the amount of melted Si. Indeed, for an ED of 0.675 J/cm², Rs starts to increase for multilayers, while it is minimum for lower ED. For the same ED (0.675 J/cm²), the Rs of reference samples starts to decrease (Fig. 15). It means that c-Si starts to melt for this ED leading to the favorable microstructure after UV-NLA and finally to the formation of the C54-$TiSi_2$ phase after RTA. It thus seems that for ED between 0.575 and 0.650 J/cm², only a-Si is melted while for ED = 0.675 J/cm² and above, c-Si starts to melt, resulting in a less favorable microstructure after UV-NLA and thus a mixing of two phases instead of only the C54-$TiSi_2$ phase.

Similarly, for both types of samples and for ED equal or higher than 0.750 J/cm², the C54-$TiSi_2$ phase is not the only silicide phase that is formed or is even not formed at all. In both cases, the explanation might be the same: the large amount of c-Si that melts during the UV-NLA prevents the formation of an amorphous Ti_xSi_{1-x} matrix containing C40-$TiSi_2$ grains, and, by extension, the formation of only the C54-$TiSi_2$ phase.

Whatsoever, the use of multilayers made of a-Si enables to reduce the UV-NLA energy density and extend the range over which only C54-$TiSi_2$ only is obtained. The reduction of ED makes UV-NLA in combination with RTA attractive to fabricate contacts since high ED may be detrimental to devices [44]. The process using multilayer is thus more reliable compared to the single ED found for reference samples and the equivalent samples by Esposito et al. [42-44]

5. Conclusion

The formation of titanium silicide using UV-NLA and a subsequent c-RTA was studied by Rs, XRD, TRR, SEM and TEM-EDX. Results showed that the formation of the C54-$TiSi_2$ phase using UV-NLA and c-RTA on TiN / a-Si / Ti / a-Si / c-Si (substrate) multilayers was possible with a lower overall thermal budget than with a classical TiN / Ti deposition. The minimum UV-NLA energy density resulting in the formation of the C54-$TiSi_2$ phase was indeed reduced from 0.675 J/cm² for a “classical” deposition without a-Si to 0.575 J/cm² for multilayers. After UV-NLA, the c-RTA temperature required to form C54-$TiSi_2$ was also reduced from 650 °C for reference samples to 600 °C for multilayers. Furthermore, the ED process window over which the C54-$TiSi_2$ phase was obtained was larger with multilayers than with reference samples without a-Si. Indeed, the C54-$TiSi_2$ phase can be obtained between 0.575 J/cm² and 0.725 J/cm² for multilayers after 3 UV-NLA pulses and a subsequent c-RTA at 600 °C. These results are explained by the possible formation of a favorable microstructure, i.e. C40-$TiSi_2$ grains embedded in a matrix of amorphous silicide, that can be formed with the appropriate laser annealing conditions and that promote the formation of only the C54-$TiSi_2$ phase at lower RTA temperature resulting in a strong Rs decrease. This

favorable microstructure can be obtained at lower ED and for a wider ED range in the multilayer samples. This is due to the limited amount of a-Si and to the lower melting temperature of a-Si that was confirmed by the appearance of wrinkles at the surface, as observed by SEM, and the increase of in-situ reflectivity as well as simulations of the temperature evolution during UV-NLA. These experiments and simulations evidenced a transient liquid phase resulting upon solidification in the microstructure favorable to the formation of the C54-$TiSi_2$ phase. TEM-EDX measurements otherwise revealed the presence of pores filled with Ar due to the a-Si deposition process.

Credit authorship contribution statement.

Réda Guelladress: Writing – original draft, Methodology, Investigation, Conceptualization, Visualization. **Sébastien Kerdilès:** Writing – review & editing, Supervision, Methodology, Conceptualization. **Melanie Dartois**: Resources. **Chiara Sabbione:** Resources. **Magali Gregoire:** Writing – review & editing, Supervision, Methodology, Conceptualization, Funding acquisition. **Dominique Mangelinck:** Writing – review & editing, Supervision, Methodology, Conceptualization, Funding acquisition, Software.

Declaration of competing interest

The authors declare that they have no known competing financial interests or personal relationships that could have appeared to influence the work reported in this paper. This research did not receive any specific grant from funding in the public, commercial, or not-for-profit sectors.

Data availability

Data will be made available on request.

References

[1] C. Lavoie, P. Adusumilli, A. V. Carr, J. S. Jordan Sweet, A. S. Ozean, E. Levrau, N. Beil, E. Alptekin, Contacts in advanced CMOS History and emerging challenges, ECS Transactions (2017), 77, 59. https://doi.org/10.1149/07705.0059ecst

[2] K. Maex, Silicides for integrated circuits: TiSi2 and CoSi2, Mater. Sci. Eng. R 11, 7 (1993). https://doi.org/10.1016/0927-796X(93)90001-J

[3] Z. Ma, Y. Xu, L.H. Allen, and S. Lee, Nucleation and growth in the initial stage of metastable titanium disilicide formation, J. Appl. Phys. 74, 2954 (1993). http://dx.doi.org/10.1063/1.354602

[4] A. Mouroux and S. L. Zhang, Alternative pathway for the formation of C54-TiSi2, J. Appl. Phys. 86, 704 (1999). https://doi.org/10.1063/1.370789

[5] L.A. Clevenger and R.W. Mann, The C49 to C54 Phase Transformation in TiSi2 Thin Films, J. Electrochem. Soc. 141, 1347 (1994). DOI 10.1149/1.2054921

[6] Z. Ma, L.H. Allen, and D.D.J. Allman, Microstructural aspects and mechanism of the C49-$TiSi_2$ to C54-$TiSi_2$ polymorphic transformation in titanium disilicide, J. Appl. Phys. 77, 4384 (1995). http://dx.doi.org/10.1063/1.359464

[7] P. Adusumilli, A. V. Carr, A.S. Ozcan, C. Lavoie, J. Jordan-Sweet, D. Prater, N. Breil, S. Polvino, M. Raymond, D. Deniz, and V. Kamineni, Formation and Microstructure of Thin Ti Silicide Films for Advanced Technologies, 2016 IEEE Int. Interconnect Technol. Conf. / Adv. Met. Conf. IITC/AMC 2016 139 (2016). http://dx.doi.org/10.1109/IITC-AMC.2016.7507710

[8] S.A. Chew, H. Yu, M. Schaekers, S. Demuynck, G. Mannaert, E. Kunnen, E. Rosseel, A. Hikavyy, A. Dangol, K. De Meyer, D. Mocuta, N. Horiguchi, G. Leusink, C. Wajda, T. Hakamata, T. Hasegawa, K. Tapily, and R. Clark, Ultralow Resistive Wrap Around Contact to Scaled FinFET Devices by using ALD-Ti Contact Metal, IITC 2017 - 2017 IEEE Int. Interconnect Technol. Conf. 5 (2017). http://dx.doi.org/10.1109/IITC-AMC.2017.7968969

[9] C.P. Chou, C.Y. Chen, K.Y. Chen, S.C. Teng, J.H. Huang, and Y.H. Wu, Improved Current Drivability for Sub-20-nm N-FinFETs by Ge Pre-Amorphization in Contact With Reverse Retrograde Profile, IEEE Electron Device Lett. 38, 299 (2017). http://dx.doi.org/10.1109/LED.2017.2647957

[10] R.A. Roy, C. Cabral Jr., and C. Lavoie, The future of silicide for CMOS contacts, Mater. Res. Soc. Symp. Proc. 564, 35 (1999). https://doi.org/10.1557/PROC-564-35

[11] M. Grégoire, B. Horvat, B.N. Bozon, D. Combe, K. Dabertrand, and D. Roy, Additional Siconi™ pre-clean for reliable TiSix contacts in advanced imager technologies, Micro Nano Eng. 2 104 (2019). https://doi.org/10.1016/j.mne.2019.02.001

[12] S. Mao and J. Luo, Titanium-based ohmic contacts in advanced CMOS technology, J. Phys. D. Appl. Phys. 52, (2019). http://dx.doi.org/10.1088/1361-6463/ab3dc9

[13] C. Fenouillet-Beranger et al., FDSOI bottom MOSFETs stability versus top transistor thermal budget featuring 3D monolithic integration, Solid-State Electronics 113, pp. 2-8 (2015). http://dx.doi.org/10.1016/j.sse.2015.05.005

[14] Cavalcante et al., 28nm FDSOI CMOS technology (FEOL and BEOL) thermal stability for 3D Sequential Integration: yield and reliability analysis, IEEE symposium on VLSI technology, vol. 1, pp. 3–4 (2020). http://dx.doi.org/10.1109/VLSITechnology18217.2020.9265075

[15] M. Gregoire, F. Morris Anak, S. Verdier, K. Dabertrand, S. Guillemin, D. Mangelinck, On the influence of Ni(Pt)Si thin film formation on agglomeration threshold temperature and its impact on 3D imaging technology integration, Microelectronic Engineering, Volumes 271–272, (2023). https://doi.org/10.1016/j.mee.2023.111937

[16] D. Mangelinck, J.Y. Dai, J.S. Pan, and S.K. Lahiri, Enhancement of thermal stability of NiSi films on (100)Si and (111)Si by Pt addition, Appl. Phys. Lett. 75, 1736-1738 (1999). https://doi.org/10.1063/1.124803.

[17] C. Lavoie et al., Towards implementation of a nickel silicide process for CMOS technologies, MEE, issues 2-4, 144-157 (2003). https://doi.org/10.1016/S0167-9317(03)00380-0

[18] P. S. Lee et al., On the Morphological Changes of Ni- and Ni(Pt)-Silicides, JES (2005). http://dx.doi.org/10.1149/1.1862255

[19] P. Ahmet et al., Thermal stability of Ni silicide films on heavily doped n+ and p+ Si substrates, MEE, 1642–1646 (2008). https://doi.org/ 10.1016/j.mee.2008.04.001

[20] K. De Keyser et al., Phase formation and thermal stability of ultrathin nickel-silicides on Si(100) APL 96, 17 (2010). https://doi.org/ 10.1063/1.3384997

[21] F. Geenen et al., Controlling the formation and stability of ultra-thin nickel silicides - an alloying strategy for preventing agglomeration, JAP, 075303 (2018). https://doi.org/10.1063/1.5009641

[22] T. Luo et al., Role of the slow diffusion species in the dewetting of compounds: the case of NiSi on a Si isotope multilayer studied by atom probe tomography, Acta M., volume 165, 192-202 (2019). https://doi.org/10.1016/j.actamat.2018.11.042

[23] D. Deduytsche, C. Detavernier, R.L. Van Meirhaeghe, and C. Lavoie, High-temperature degradation of NiSi films: agglomeration versus NiSi2 nucleation, J. Appl. Phys. 98, (2005). https://doi.org/10.1063/1.2005380

[24] C. Lavoie, C. Detavernier, C. Cabral, F.M. d'Heurle, A.J. Kellock, J. Jordan-Sweet, and J.M.E. Harper, Effects of additive elements on the phase formation and morphological stability of nickel monosilicide films, Microelectron. Eng. 83, 2042 (2006). https://doi.org/10.1016/j.mee.2006.09.006.

[25] M. Gregoire, R. Beneyton and P. Morin, Millisecond annealing for salicide formation: Challenges of NiSi agglomeration free process, IEEE Int. Interconnect Technol. Conf. 2011 Mater. Adv. Met. IITC/MAM, pp. 1–3 (2011) https://doi. org/10.1109/IITC.2011.5940280

[26] T.C. Hsiao, P. Liu, and J.C.S. Woo, An Advanced Ge Pre-Amorphization Salicide Technology for Sub-Quarter Micrometer SOI CMOS Devices, Dig. Tech. Pap., Symp. VLSI Technol. 95 (1997). https://doi.org/10.1109/VLSIT.1997.623712

[27] Q. Xu and C. Hu, New Ti-SALICIDE Process Using Sb and Ge Preamorphization for Sub-0.2 m CMOS Technology, IEEE Trans. Electron Devices 45, 2002-2009 (1998). http://dx.doi.org/10.1109/16.711367

[28] H. Yu, M. Schaekers, E. Rosseel, A. Peter, J.G. Lee, W.B. Song, S. Demuynck, T. Chiarella, J.A. Ragnarsson, S. Kubicek, J. Everaert, N. Horiguchi, K. Barla, D. Kim, N. Collaert, A.V.Y. Thean, and K. De Meyer, 1.5×10-9 ὸ·cm2 Contact Resistivity on Highly Doped Si:P Using Ge Pre-amorphization and Ti Silicidation, Tech. Dig. - Int. Electron Devices Meet. 21.7.1 (2015). http://dx.doi.org/10.1109/IEDM.2015.7409753

[29] J.U. Bae, D.K. Sohn, J.S. Park, B.H. Lee, C.H. Han, and J.W. Park, Effect of pre-amorphization of polycrystalline silicon on agglomeration of in subquarter micron Si lines, J. Appl. Phys. 86, 4943 (1999). http://dx.doi.org/10.1063/1.371523

[30] S.M. Chang, H.Y. Huang, H.Y. Yang, L.J. Chen, Mechanism of enhanced formation of C54–$TiSi_2$ in high-temperature deposited Ti thin films on preamorphized (001) Si Appl. Phys. Lett. 74, 224, (1999). https://doi.org/10.1063/1.123300

[31] P. Revesz, J. Gyimesi, and E. Zsoldos, Growth of titanium silicide on ion-implanted silicon, J. Appl. Phys., vol. 54, no. 4, p. 1860, (1983). http://dx.doi.org/10.1063/1.332237

[32] A. Mouroux, M. Roux, S.L. Zhang, F.M. D'Heurle, C. Cabral, C. Lavoie, and J.M.E. Harper, Phase formation and resistivity in the ternary system Ti–Nb–Si, J. Appl. Phys. 86, 2323 (1999). https://doi.org/10.1063/1.371049

[33] A. Mouroux, S.L. Zhang, W. Kaplan, S. Nygren, M. Östling, and C.S. Petersson, Enhanced formation of the C54 phase of $TiSi_2$ by an interposed layer of molybdenum, Appl. Phys. Lett. 69, 975 (1996). http://dx.doi.org/10.1063/1.117100

[34] Y.C. Peng, L.J. Chen, W.Y. Hsieh, Y.R. Yang, and Y.F. Hsieh, Enhancement of C-49 to C54-TiSi2 phase transformation on (001) Si with an ultrathin TiN seed layer, Appl. Surf. Sci. 142, 336-340 (1999). https://doi.org/10.1016/S0169-4332(98)00671-0

[35] S.Y. Chen, Z.X. Shen, Z.D. Chen, A.K. See, L.H. Chan, T.J. Zhang, and K.C. Tee, Laser-induced Formation of Titanium Silicides, Surf. Interface Anal. 28, 200-203 (1999). https://doi.org/10.1002/(SICI)1096-9918(199908)28:1%3C200::AID-SIA607%3E3.0.CO;2-2

[36] Y.F. Chong, K.L. Pey, A.T.S. Wee, A. See, Z.X. Shen, C.H. Tung, R. Gopalakrishnan, and Y.F. Lu, Laser-induced titanium disilicide formation for submicron technologies, J. Electron. Mater. 30, 1549 (2001). https://ui.adsabs.harvard.edu/link_gateway/2001JEMat..30.1549C/doi:10.1007/s11664-001-0172-2

[37] S.Y. Chen, Z.X. Shen, Z.D. Chen, L.H. Chan, and A.K. See, Laser-induced direct formation of C54-$TiSi_2$ films with fine grains on c-Si substrates, Appl. Phys. Lett. 75, 1727-1729 (1999). http://dx.doi.org/10.1063/1.124801

[38] L. Lu and M.O. Lai, Laser induced transformation of $TiSi_2$, J. Appl. Phys. 94, 4291 (2003). DOI: 10.1063/1.1606111

[39] S.Y. Chen, Z.X. Shen, K. Li, A.K. See, and L.H. Chan, Synthesis and characterization of pure C40-$TiSi_2$, Appl. Phys. Lett. 77, 4395 (2000). http://dx.doi.org/10.1063/1.1329864

[40] S.Y. Chen, Z.X. Shen, A.K. See, and L.H. Chan, Enhancement Effect of C40-$TiSi_2$ on the C54 Phase Formation, J. Electrochem. Soc. 148, 734 (2001). DOI 10.1149/1.1417978

[41] S.Y. Chen, Z.X. Shen, S.Y. Xu, C.K. Ong, A.K. See, and L.H. Chan, Excimer laser-induced Ti silicidation to eliminate the fine-line effect for integrated circuit device fabrication, J. Electrochem. Soc. 149, 609 (2002). DOI 10.1149/1.1510843

[42] L. Esposito, Mise en œuvre de procédés innovants pour l'optimisation de contacts TiSi pour les technologies imageurs avancées, PhD thesis, Aix-Marseille Université (2021).

[43] L. Esposito, S. Kerdilès, M. Gregoire, P. Benigni, K. Dabertrand, J-G. Mattei, D. Mangelinck, impact of nanosecond laser energy density on the C40-$TiSi_2$ formation and C54-$TiSi_2$ transformation temperature, Journal of Applied Physics, American Institute of Physics, 128 (8), pp.085305 (2020). http://aip.scitation.org/doi/10.1063/5.0016091

[44] L. Esposito, S. Kerdilès, M. Gregoire, D. Mangelinck, Impact of Nanosecond Laser Annealing on the Formation of Titanium Silicides. 2021 20th International Workshop on Junction Technology (IWJT), Kyoto, France. pp.1-6 (2021). http://dx.doi.org/10.23919/IWJT52818.2021.9609410

[45] H. Allam, Développement de matériaux cimentaires fibrés multifonctionnels type « smart concrete », PhD thesis, Aix-Marseille Université, 2020

[46] K. Huet, J. Aubin, P.E. Raynal, B. Curvers, A. Verstraete, B. Lespinasse, F. Mazzamuto, A. Sciuto, S.F. Lombardo, A. La Magna, P. Acosta-Alba, L. Dagault, C. Licitra, J.M. Hartmann,

and S. Kerdilès, Pulsed laser annealing for advanced technology nodes: modeling and calibration, Appl. Surf. Sci. 505, 144470 (2020). https://doi.org/10.1016/j.apsusc.2019.144470

[47] A. La Magna, P. Alippi, V. Privitera, G. Fortunato, M. Camalleri, and B. Svensson, A phase-field approach to the simulation of the excimer laser annealing process in Si, J. Appl. Phys. 95, 4806-4814 (2004). http://dx.doi.org/10.1063/1.1690861

[48] G. Fisicaro and A. La Magna, Modeling of laser annealing, J. Comput. Electron. 13, 70 (2014). DOI 10.1007/s10825-013-0545-9 :

[49] J. Boneberg and P. Leiderer, On the Interpretation of Time-Resolved Surface Reflectivity Measurements during the Laser Annealing of Si Thin Films, Phys. Status Solidi A 166, 643 (1998). https://doi.org/10.1002/(SICI)1521-396X(199804)166:2%3C643::AID-PSSA643%3E3.0.CO;2-L

[50] L. Benaissa and J.-S. Moulet, Method for manufacturing nanometric objects using the rupture of a layer deformed by wrinkles, European Patent Office. (2020) EP3058584 .

[51] J.F. Cornet. Résolution des équations de l'effet Kirkendall. Revue de Physique Appliquée, 8 (4), pp.293-305 (1973). https://dx.doi.org/10.1051/rphysap:0197300804029300